CLEO CONF 96-3
ICHEP96 PA05-078

Measurement of $\mathcal{B}(\bar{B}^0 \to D^+\ell^-\bar{\nu})$ and Extraction of $|V_{cb}|$

CLEO Collaboration

(July 9, 1996)

Abstract

Using data taken with the CLEO detector at CESR, we use two methods to measure the exclusive decay rate of $\bar{B}^0 \to D^+\ell^-\bar{\nu}$ and its dependence on the HQET variable w. Our preliminary result is $\mathcal{B}(\bar{B}^0 \to D^+\ell^-\bar{\nu}) = (1.78 \pm 0.20 \pm 0.24)\%$. From a fit to the differential decay distribution we obtain a value of $|V_{cb}\mathcal{F}(w=1)| = (3.46 \pm 0.42 \pm 0.46) \times 10^{-2}$. We compare the results obtained in this analysis to previous results obtained for the decay $\bar{B}^0 \to D^{*+}\ell^-\bar{\nu}$.

T. Bergfeld,[1] B.I. Eisenstein,[1] J. Ernst,[1] G.E. Gladding,[1] G.D. Gollin,[1] E. Johnson,[1] I. Karliner,[1] M. Palmer,[1] M. Selen,[1] J.J. Thaler,[1] K.W. Edwards,[2] A. Bellerive,[3] D.I. Britton,[3] R. Janicek,[3] D.B. MacFarlane,[3] K.W. McLean,[3] P.M. Patel,[3] A.J. Sadoff,[4] R. Ammar,[5] P. Baringer,[5] A. Bean,[5] D. Besson,[5] D. Coppage,[5] R. Davis,[5] N. Hancock,[5] S. Kotov,[5] I. Kravchenko,[5] N. Kwak,[5] S. Anderson,[6] Y. Kubota,[6] M. Lattery,[6] J.J. O'Neill,[6] S. Patton,[6] R. Poling,[6] T. Riehle,[6] A. Smith,[6] V. Savinov,[6] M.S. Alam,[7] S.B. Athar,[7] Z. Ling,[7] A.H. Mahmood,[7] H. Severini,[7] S. Timm,[7] F. Wappler,[7] A. Anastassov,[8] S. Blinov,[8a] J.E. Duboscq,[8] R. Fulton,[8] D. Fujino,[8] K.K. Gan,[8] T. Hart,[8] K. Honscheid,[8] H. Kagan,[8] R. Kass,[8] J. Lee,[8] M. Sung,[8] A. Undrus,[8a] R. Wanke,[8] A. Wolf,[8] M.M. Zoeller,[8] B. Nemati,[9] S.J. Richichi,[9] W.R. Ross,[9] P. Skubic,[9] M. Wood,[9] M. Bishai,[10] J. Fast,[10] E. Gerndt,[10] J.W. Hinson,[10] D.H. Miller,[10] E.I. Shibata,[10] I.P.J. Shipsey,[10] M. Yurko,[10] L. Gibbons,[11] S.D. Johnson,[11] Y. Kwon,[11] S. Roberts,[11] E.H. Thorndike,[11] C.P. Jessop,[12] K. Lingel,[12] H. Marsiske,[12] M.L. Perl,[12] S.F. Schaffner,[12] D. Ugolini,[12] R. Wang,[12] X. Zhou,[12] T.E. Coan,[13] V. Fadeyev,[13] I. Korolkov,[13] Y. Maravin,[13] I. Narsky,[13] V. Shelkov,[13] R. Stroynowski,[13] J. Staeck,[13] I. Volobouev,[13] J. Ye,[13] M. Artuso,[14] A. Efimov,[14] M. Gao,[14] M. Goldberg,[14] R. Greene,[14] F. Frasconi,[14] D. He,[14] S. Kopp,[14] G.C. Moneti,[14] R. Mountain,[14] Y. Mukhin,[14] S. Schuh,[14] T. Skwarnicki,[14] S. Stone,[14] X. Xing,[14] J. Bartelt,[15] S.E. Csorna,[15] V. Jain,[15] S. Marka,[15] A. Freyberger,[16] R. Godang,[16] D. Gibaut,[16] K. Kinoshita,[16] I.C. Lai,[16] P. Pomianowski,[16] S. Schrenk,[16] G. Bonvicini,[17] D. Cinabro,[17] L. Perera,[17] B. Barish,[18] M. Chadha,[18] S. Chan,[18] G. Eigen,[18] J.S. Miller,[18] C. O'Grady,[18] M. Schmidtler,[18] J. Urheim,[18] A.J. Weinstein,[18] F. Würthwein,[18] D.M. Asner,[19] D.W. Bliss,[19] W.S. Brower,[19] G. Masek,[19] H.P. Paar,[19] J. Gronberg,[20] D.J. Lange,[20] C.M. Korte,[20] R. Kutschke,[20] S. Menary,[20] R.J. Morrison,[20] S. Nakanishi,[20] H.N. Nelson,[20] T.K. Nelson,[20] C. Qiao,[20] J.D. Richman,[20] D. Roberts,[20] A. Ryd,[20] H. Tajima,[20] M.S. Witherell,[20] R. Balest,[21] B.H. Behrens,[21] K. Cho,[21] W.T. Ford,[21] H. Park,[21] P. Rankin,[21] J. Roy,[21] J.G. Smith,[21] J.P. Alexander,[22] C. Bebek,[22] B.E. Berger,[22] K. Berkelman,[22] K. Bloom,[22] D.G. Cassel,[22] H.A. Cho,[22] D.M. Coffman,[22] D.S. Crowcroft,[22] M. Dickson,[22] P.S. Drell,[22] R. Ehrlich,[22] R. Elia,[22] A.D. Foland,[22] P. Gaidarev,[22] B. Gittelman,[22] S.W. Gray,[22] D.L. Hartill,[22] B.K. Heltsley,[22] P.I. Hopman,[22] S.L. Jones,[22] J. Kandaswamy,[22] N. Katayama,[22] P.C. Kim,[22] D.L. Kreinick,[22] T. Lee,[22] Y. Liu,[22] G.S. Ludwig,[22] J. Masui,[22] J. Mevissen,[22] N.B. Mistry,[22] C.R. Ng,[22] E. Nordberg,[22] M. Ogg,[22b] J.R. Patterson,[22] D. Peterson,[22] D. Riley,[22] A. Soffer,[22] C. Ward,[22] P. Avery,[23] M. Athanas,[23] C.D. Jones,[23] M. Lohner,[23] C. Prescott,[23] S. Yang,[23] J. Yelton,[23] G. Brandenburg,[24] R.A. Briere,[24] D. Kim,[24] T. Liu,[24] M. Saulnier,[24] R. Wilson,[24] H. Yamamoto,[24] T. E. Browder,[25] F. Li,[25] Y. Li,[25] and J. L. Rodriguez[25]

[1] *University of Illinois, Champaign-Urbana, Illinois, 61801*
[2] *Carleton University, Ottawa, Ontario K1S 5B6 and the Institute of Particle Physics, Canada*
[3] *McGill University, Montréal, Québec H3A 2T8 and the Institute of Particle Physics, Canada*
[4] *Ithaca College, Ithaca, New York 14850*
[5] *University of Kansas, Lawrence, Kansas 66045*
[6] *University of Minnesota, Minneapolis, Minnesota 55455*
[7] *State University of New York at Albany, Albany, New York 12222*

[a] Permanent address: BINP, RU-630090 Novosibirsk, Russia
[b] Permanent address: University of Texas at Austin

[8] Ohio State University, Columbus, Ohio, 43210
[9] University of Oklahoma, Norman, Oklahoma 73019
[10] Purdue University, West Lafayette, Indiana 47907
[11] University of Rochester, Rochester, New York 14627
[12] Stanford Linear Accelerator Center, Stanford University, Stanford, California, 94309
[13] Southern Methodist University, Dallas, Texas 75275
[14] Syracuse University, Syracuse, New York 13244
[15] Vanderbilt University, Nashville, Tennessee 37235
[16] Virginia Polytechnic Institute and State University, Blacksburg, Virginia 24061
[17] Wayne State University, Detroit, Michigan 48202
[18] California Institute of Technology, Pasadena, California 91125
[19] University of California, San Diego, La Jolla, California 92093
[20] University of California, Santa Barbara, California 93106
[21] University of Colorado, Boulder, Colorado 80309-0390
[22] Cornell University, Ithaca, New York 14853
[23] University of Florida, Gainesville, Florida 32611
[24] Harvard University, Cambridge, Massachusetts 02138
[25] University of Hawaii at Manoa, Honolulu, HI 96822

1 Introduction

Semileptonic B decays play a central role in our understanding of heavy quark dynamics and in determining parameters of the CKM matrix [1, 2]. Although much attention has been given to the pseudoscalar to vector transition $B \to D^* \ell^- \bar{\nu}$, little has been paid to the pseudoscalar to pseudoscalar transition $B \to D \ell^- \bar{\nu}$. Previous published analyses have made only crude measurements of the branching ratio [3] and only recently has clean reconstruction of the $D\ell^-\bar{\nu}$ decay mode been possible [4].

In this paper we present results from two independent analyses of the $\bar{B}^0 \to D^+ \ell^- \bar{\nu}$ decay [5]. One analysis uses a neutrino reconstruction method that takes advantage of the hermeticity of the CLEO detector to infer the 4-momentum of the undetected neutrino and extracts the signal using full reconstruction of the semileptonic decay. The other analysis takes advantage of the fact that B mesons produced in the decay of the $\Upsilon(4S)$ are almost at rest and isolates a signal with a missing mass technique. The advantage of the first analysis is low background ($S/N \approx 1/1$ *vs.* $S/N \approx 1/25$), while the advantage of the second analysis is high efficiency ($\epsilon \approx 12.5\%$ *vs.* $\epsilon \approx 2.5\%$).

From the differential decay rate $d\Gamma(\bar{B}^0 \to D^+ \ell^- \bar{\nu})/dw$, where $w = v \cdot v'$ is the dot product of the four-velocities of the initial and final mesons, both analyses extract $\mathcal{F}(1)|V_{cb}|$ within the framework of HQET, where the $w = 1$ limit of the form factor $\mathcal{F}(w)$ is model dependent. Both analyses also extract values of $|V_{cb}|$ from fits to the $d\Gamma/dq^2$ distribution using a variety of parameterizations of the form factor for the decay, and the value of $d\Gamma/dq^2$ at $q^2 = m_\pi^2$ and m_ρ^2 is used to test the hypothesis of factorization for B decays into $D^+\pi^-$ and $D^+\rho^-$ final states.

Our data sample consists of $B\bar{B}$ pairs which are produced in e^+e^- collisions at the $\Upsilon(4S)$ resonance collected by the CLEO detector at the Cornell Electron Storage Ring (CESR). The neutrino reconstruction analysis uses 2.63×10^6 $B\bar{B}$ pairs corresponding to an integrated luminosity of 2.46 fb^{-1}, while the missing mass analysis uses 2.15×10^6 $B\bar{B}$ pairs corresponding to an integrated luminosity of 2.02 fb^{-1}. In this environment, the $B\bar{B}$ system is at rest, and the B meson energy is the same as the beam energy E_{beam}. We assume equal production of B^+B^- and $B^0\bar{B}^0$ from the $\Upsilon(4S)$. The detector is described in detail elsewhere [6], but for this analysis we note that it has excellent hermeticity and angular coverage. Three concentric tracking devices provide a momentum resolution of $(\sigma_p/p)^2 = (0.005)^2+(0.0015p)^2$ (p in GeV/c), while covering 95% of the 4π solid angle. The CsI calorimeter located inside of the CLEO solenoid covers 98% of 4π and provides an energy resolution well approximated by $\sigma_E/E = 0.019 + 0.0035/E^{0.75} - 0.001E$ (E in GeV) in the region $|\cos\theta| < 0.71$, where θ is polar angle measured from the beam axis.

2 $\bar{B}^0 \to D^+\ell^-\bar{\nu}$ via Neutrino Reconstruction

2.1 Analysis Method

The neutrino in the decay $\bar{B}^0 \to D^+\ell^-\bar{\nu}$ cannot be detected directly. However, the neutrino momentum vector can be inferred from other information available in the event. Once the neutrino momentum vector is known, the $\bar{B}^0$ can be fully reconstructed.

In this analysis, we reconstruct the neutrino four-momentum by measuring the momentum and energy missing from each event. We define

$$\begin{aligned} E_{miss} &\equiv 2E_{beam} - \sum_i E_i \\ \vec{p}_{miss} &\equiv -\sum_i \vec{p}_i, \end{aligned} \tag{1}$$

where the index i runs over all legitimate charged tracks and calorimeter showers. To obtain an accurate measurement of E_{miss} and $\vec{p}_{miss}$, we have developed algorithms to reject fake tracks and clusters from the events. Good resolution for the unobserved neutrino can only be achieved in events with very few missing particles. Therefore, we make requirements on event quality to remove events with missing particles in addition to the neutrino. We remove events with more than one lepton, since they indicate additional missing neutrinos. We also make a requirement on the net charge of the event. Only events with net charge of 0 or ± 1 are used; net charge of ± 1 is allowed for increased selection efficiency.

Events with other missing particles, such as K_L^0 mesons, are substantially reduced by requiring that the missing mass in the event, $MM_{EV}^2 \equiv E_{miss}^2 - |\vec{p}_{miss}|^2$, be consistent with zero. We require $-450 \leq MM_{EV}^2/2E_{miss} \leq 300$ MeV, since the resolution on MM_{EV}^2 varies roughly as $2E_{miss}\sigma_{E_{miss}}$. We have achieved resolutions of approximately 260 MeV on E_{miss} and 110 MeV/c on $\vec{p}_{miss}$ in events that do not contain K_L^0 particles or additional neutrinos. Because $|\vec{p}_{miss}|$ has better resolution than E_{miss}, we use it as a measure of the neutrino energy.

For this analysis we select hadronic events that have at least one track identified as a lepton. Electrons are identified through specific ionization, energy and momentum measurements, and position matching between the tracking and calorimeter systems. We accept electron candidates with momenta greater than 0.8 GeV/c and $|\cos\theta| < 0.91$, where θ is the

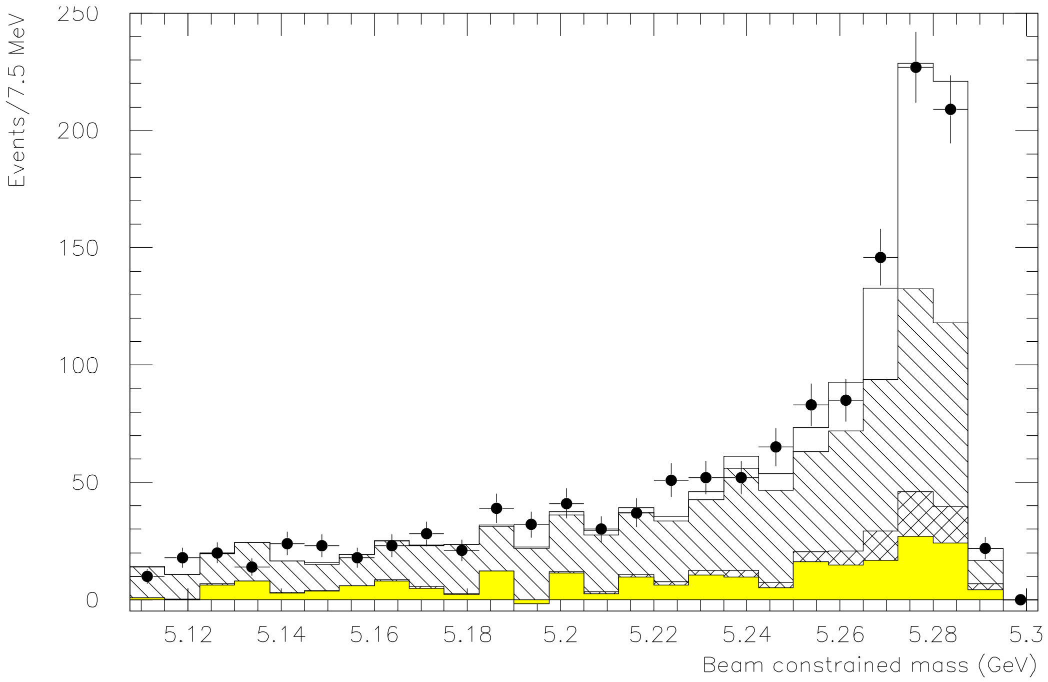

Figure 1: Beam constrained mass spectrum for all events passing the cuts described in the text (points). The white area represents the signal events, the hatched area represents the combinatoric background, the crosshatched area represents the $\bar{B}^0 \to D^{+*}\ell^-\bar{\nu}$ background, and the shaded area represents all the remaining backgrounds, as described in the text.

angle of the electron-candidate direction with respect to the beam axis. Muons are identified through hits in muon counters at a depth of five interaction lengths, limiting muon candidates to momenta greater than 1.4 GeV/c, and to the region $|\cos\theta| < 0.87$. In order to suppress events from continuum production of quark-antiquark pairs, we require that the ratio of the Fox-Wolfram [7] moments, H_2/H_0, be less than 0.4.

We search for D^+ candidates in the decay mode $D^+ \to K^-\pi^+\pi^+$, where we require the measured specific ionization for the D^+ daughters to be consistent with the assumed particle hypothesis. D^+ candidates are required to have an invariant mass of $1.855 \leq M_{K\pi\pi} \leq 1.885$ GeV. Since the D^+ must come from a B decay, we also require $|\vec{p}_{K\pi\pi}|/\sqrt{(E^2_{beam} - M^2_{D^+})} < 0.5$. For this analysis, we wish to eliminate any D^+ candidates that are daughters of D^{*+} decays. In each event the candidate D^+ is paired with neutral pions to form candidate D^{*+} mesons. If the candidate $D^* - D$ mass difference is within 3 MeV of the nominal value, we reject the event.

$\bar{B}^0 \to D^+\ell^-\bar{\nu}$ candidates are selected through a full reconstruction of the B. The energy difference $\Delta E \equiv E_{beam} - (E_{D^+} + E_\ell + |\vec{p}_{miss}|)$ should be zero, and the beam constrained mass $M_B \equiv \sqrt{E^2_{beam} - |\vec{p}_{D^+} + \vec{p}_\ell + \vec{p}_{miss}|^2}$ should be equal to the B mass. In this analysis, we require $-500 \leq \Delta E \leq 100$ MeV. The ΔE cut is asymmetric because of $B \to D^*\ell\nu$ backgrounds that are present at higher ΔE. Figure 1 shows the beam constrained mass distribution for events passing all of the above cuts. The signal region is $5.2650 \leq M_B < 5.2875$ GeV. The yield in the signal region is 582 events.

2.2 Backgrounds

While there is a significant enhancement near the B mass in Figure 1, there are still backgrounds to be considered. We will discuss each background source individually.

2.2.1 Continuum Background

One source of background is $\ell^- D^+$ pairs from continuum production of quark-antiquark pairs. These events are represented using data taken at center-of-mass energies below the $\Upsilon(4S)$ resonance. The normalization of this background is determined by scaling this data sample to the same luminosity as the on-resonance sample, correcting for the energy dependence of the cross section. The contribution of this background to the signal region is given in Table 1, as are all the other background contributions.

2.2.2 Combinatoric Background

Another background in this analysis is the combinatoric background in the D^+ reconstruction. This background is well modeled by events passing all other analysis cuts but where the D^+ candidate mass is just outside the D^+ mass cuts. We select $1.785 \leq M_{K\pi\pi} < 1.835$ GeV and $1.905 \leq M_{K\pi\pi} < 1.955$ GeV for the sideband region. The normalization of the combinatoric background is determined by assuming that the $K\pi\pi$ invariant mass shape is linear under the signal peak, and by scaling the number of events in the sidebands to equal area under the peak. The uncertainty associated with this assumption is included in our systematic errors.

2.2.3 Correlated Background

Correlated background refers to events in which the D^+ and the lepton come from the same parent B. These events are a background to this analysis because $B \to D^{*(*)}\ell\nu$ decays are very similar to $\bar{B}^0 \to D^+\ell^-\bar{\nu}$ decays in their kinematics. In particular, because the $D^* - D$ mass difference is so small, $B \to D^*\ell\nu$ events reconstructed as $\bar{B}^0 \to D^+\ell^-\bar{\nu}$ are only slightly smeared in M_B and shifted by about 150 MeV in ΔE compared to true $\bar{B}^0 \to D^+\ell^-\bar{\nu}$ events. The contribution to the yield from $B \to D^*\ell\nu$ decays is modeled by Monte Carlo simulation, and is normalized to the measured CLEO branching fraction for $B \to D^*\ell\nu$ [8]: $\mathcal{B}(\bar{B}^0 \to D^{*+}\ell^-\nu) = (4.49 \pm 0.32 \pm 0.39)\%$.

The contributions from the $B \to D^{**}\ell\nu$ decays are subtracted in a similar way. We assume that 2.5% of B mesons decay to the narrow D^{**} states D_1 and D_2^*, and 1.1% of B mesons decay to broad $D\pi$ and $D^*\pi$ resonances. The branching fractions for the various $B \to D^{**}\ell\nu$ decays are not well known, so we attribute a large uncertainty to their contribution, which will be included in the systematic error. However, because the decay kinematics are sufficiently different from $\bar{B}^0 \to D^+\ell^-\bar{\nu}$, this contribution is relatively small.

2.2.4 Uncorrelated Background

In some cases, the lepton can be the daughter of one B meson in the event and the D^+ can be the daughter of the other B meson. Our Monte Carlo simulation is expected to model this

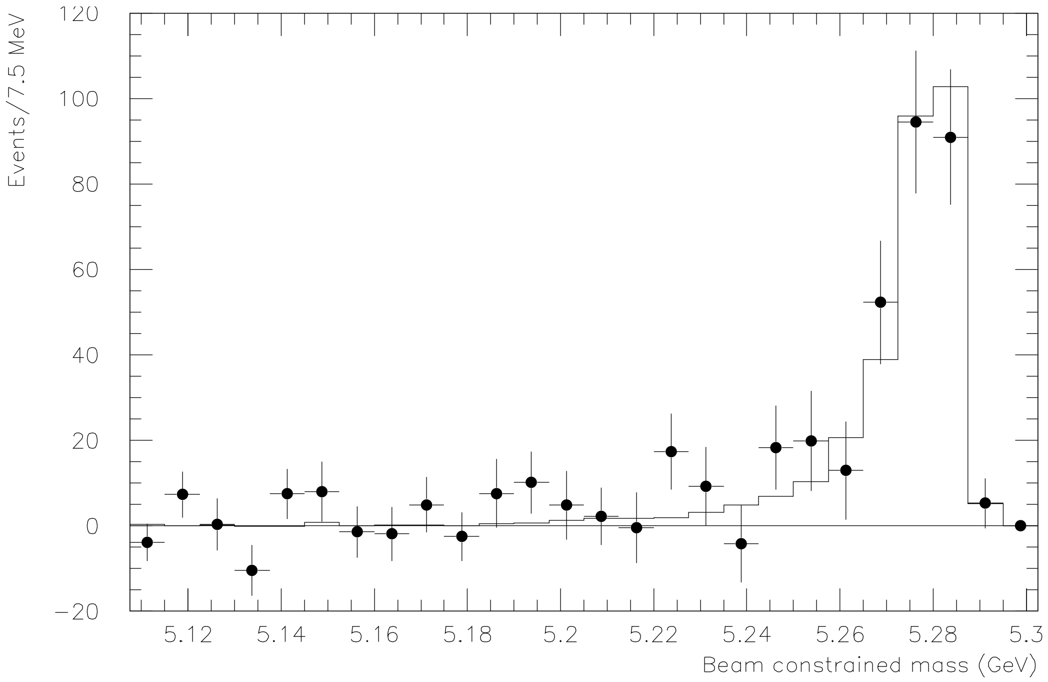

Figure 2: Beam constrained mass spectrum after all backgrounds have been subtracted (points). The histogram shows the prediction of a Monte Carlo simulation of $\bar{B}^0 \to D^+\ell^-\bar{\nu}$ decays, normalized to equal area in the signal region.

background well, because it reproduces the inclusive lepton and D^+ momentum spectra from B decays. Using the Monte Carlo, the uncorrelated background is found to be consistent with contributing no events to the signal region in this analysis.

2.2.5 Fake Lepton Background

The fake lepton background is estimated from the data. We repeat the reconstruction procedure taking tracks which fail the lepton identification requirements as leptons, and weighting their contribution by a momentum-dependent fake probability obtained from independent data samples.

Table 1 gives the numbers of events in our data sample passing all of the cuts described above, and our estimates of the various backgrounds. Figure 1 shows the contributions from the various backgrounds in the B mass signal region and Figure 2 shows the B mass distribution after all known backgrounds have been subtracted.

2.3 Results

The efficiency for reconstructing $\bar{B}^0 \to D^+\ell^-\bar{\nu}$ decays is determined using the Monte Carlo simulation. $\bar{B}^0 \to D^+\ell^-\bar{\nu}$ events are generated in the ISGW model [9] and are passed through a full detector simulation [10] and then analyzed as data. We find an efficiency for reconstructing $\bar{B}^0 \to D^+\ell^-\bar{\nu}$ decays, averaged over electrons and muons, of $\epsilon_{D^+\ell^-\bar{\nu}} = (2.63 \pm 0.01)\%$, where the error is statistical only.

Table 1: Signal and background yields from the neutrino reconstruction analysis. Errors are statistical only; the systematic errors on the background yields (not shown) are included in the summary of systematic errors.

Yields	Events
Total yield	582.0 $\pm$ 24.1
Combinatoric	229.1 $\pm$ 9.9
Continuum	27.3 $\pm$ 7.6
$\bar{B}^0 \to D^{*+}\ell^-\bar{\nu}$,$D^{*+} \to D^+\pi^0$)	47.4
Other Correlated Background	36.4
Fakes	4.0
$\bar{B}^0 \to D^+ l^- \bar{\nu}$ signal	237.8 $\pm$ 27.2

Table 2: Systematic errors in the neutrino reconstruction analysis.

Source	$\mathcal{B}(D^+\ell^-\bar{\nu})$	$\lvert\mathcal{F}(1)V_{cb}\rvert$	ρ^2
Neutrino detection	15.0%	7%	4%
$D^*\ell\nu$ backgrounds	2.2%	1%	3%
Other backgrounds	5.9%	7%	10%
Efficiency	6.1%	4%	9%
B Lifetime	–	3%	–
D branching ratio	6.6%	3%	–
Total	18.6%	12%	14%

2.3.1 Branching Ratio

From the efficiency and measured yields we can extract a product branching fraction

$$\mathcal{B}(\bar{B}^0 \to D^+\ell^-\bar{\nu})\mathcal{B}(D^+ \to K^-\pi^+\pi^+) = \frac{N_{D^+\ell^-\bar{\nu}}}{4 \times N_{\Upsilon(4S)} \times f_{+-} \times \epsilon_{D^+\ell^-\bar{\nu}}} \tag{2}$$

where $N_{\Upsilon(4S)}$ is the total number of $B\bar{B}$ pairs in our data sample, $f_{+-} \equiv \mathcal{B}(\Upsilon(4S) \to B^+B^-)$ which is taken to be 0.5, and the factor of 4 is because each $\Upsilon(4S)$ decays to a B meson pair and we are combining electrons and muons. Using $\mathcal{B}(D^+ \to K^-\pi^+\pi^+) = (9.1 \pm 0.6)\%$ [11], we find

$$\mathcal{B}(\bar{B}^0 \to D^+ l^- \bar{\nu}) = (1.89 \pm 0.22 \pm 0.35)\% \tag{3}$$

where the first error is statistical and the second is systematic. Systematic errors are summarized in Table 2.

2.3.2 Extraction of $|V_{cb}|$ in the Heavy Quark Limit

The differential decay distribution for the $\bar{B}^0 \to D^+\ell^-\bar{\nu}$ decay can be written in terms of the HQET variable w as

$$\frac{d\Gamma}{dw} = \frac{1}{\tau_B}\frac{1}{4\times N_{\Upsilon(4S)}\times f_{+-}\times\epsilon(w)_{D^+\ell^-\bar{\nu}}\times\mathcal{B}(D^+\to K^-\pi^+\pi^+)}\frac{dN_{D^+\ell^-\bar{\nu}}}{dw} \quad (4)$$

$$= \frac{G_F^2|V_{cb}|^2}{48\pi^3}(M+m)^2(m\sqrt{w^2-1})^3|h_+(w)-\frac{M-m}{M+m}h_-(w)|^2. \quad (5)$$

where M is the mass of the B meson, m is the mass of the D meson, $w \equiv v\cdot v' = \frac{M^2+m^2-q^2}{2Mm}$, and we have now introduced two HQET form factors, $h_+(w)$ and $h_-(w)$ following Reference 2. In the limit of infinitely heavy b and c quarks, $h_-(w)=0$, and $h_+(w)=\xi(w)$, the universal Isgur-Wise form factor [12] that appears in the decay distribution for any $B^{(*)}\to D^{(*)}$ semileptonic decay. In this same heavy quark limit, $\xi(1)=1$. As we move away from this limit, the corrections to $\xi(1)$ can be calculated in powers of $1/m_Q$, where m_Q is the mass of the heavy quark. What we measure, then, is a function $\mathcal{F}(w)$, which can be related to $\xi(w)$ by correction terms that disappear in the infinitely heavy quark limit. We will assume a linear shape for the form factor [8], which we take as

$$\mathcal{F}(w) \equiv h_+(w) - \frac{M-m}{M+m}h_-(w) = \mathcal{F}(1)(1-\rho^2(w-1)), \quad (6)$$

where ρ^2 is the slope of the form factor.

The decay distribution we observe is $dN/d\tilde{w}$ where N is the number of observed events and $\tilde{w}$ is the observed value of w taking into account smearing due to the inherent resolution of the detector. The smearing is small compared to the bin width of 0.06 which we use for our fit and is well represented by a double Gaussian. We fit the $dN/d\tilde{w}$ distribution with a convolution of the theoretical form of $d\Gamma/dw$ and a resolution function. We take $\tau_B = (1.58\pm0.05)$ ps. The $dN/d\tilde{w}$ distribution after efficiency correction and the result of the fit [13], is shown in Figure 3.

The results of this analysis, including systematic errors, are

$$|\mathcal{F}(1)V_{cb}| = (3.60\pm0.57\pm0.42)\times10^{-2} \quad (7)$$

$$\rho^2 = 0.73\pm0.24\pm0.10. \quad (8)$$

Contributions to the systematic error are listed in Table 2.

An alternative approach to extracting V_{cb} is to fit the $d\Gamma/dq^2$ distribution for $|V_{cb}f_+(q^2)|$ where the q^2 dependence of the form factor and its normalization are predicted by a model calculation. At $q^2=0$, we obtain a value $|V_{cb}f_+(0)| = (2.51\pm0.22\pm0.19)\times10^{-2}$.

3 $\bar{B}^0 \to D^+\ell^-\bar{\nu}$ via Missing Mass

3.1 Analysis Method

Since the B meson produced at the $\Upsilon(4S)$ is almost at rest in the laboratory, the final state $D^+\ell^-\bar{\nu}$ can be isolated using a missing mass technique where we need measure only the D^+

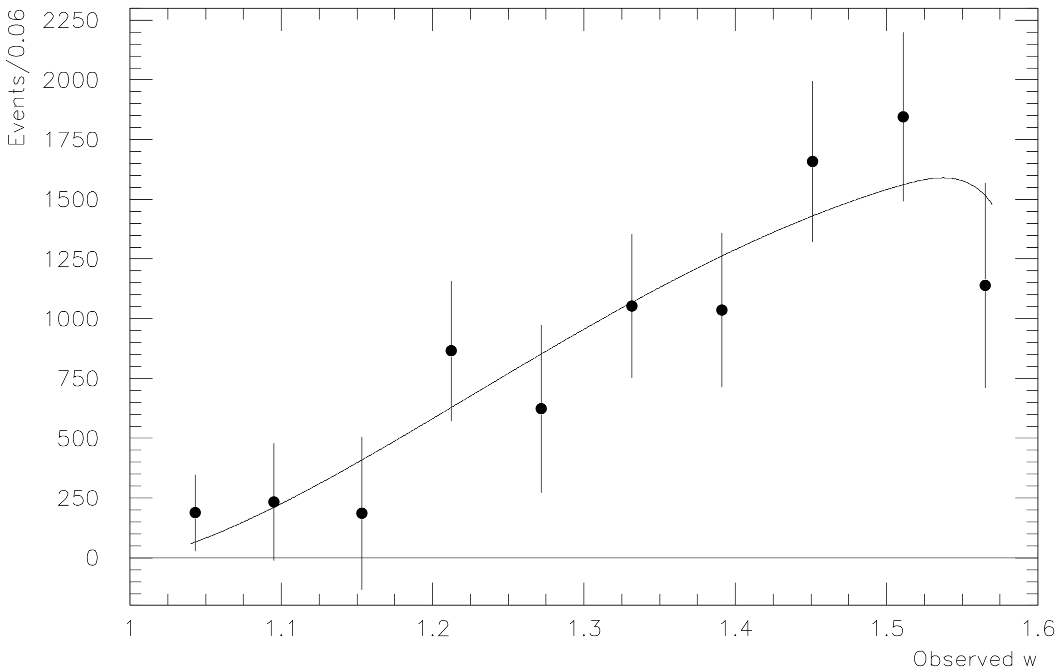

Figure 3: The result of the $dN/d\tilde{w}$ fit from the neutrino reconstruction analysis.

and the lepton. The mass squared missing from the $\bar{B}^0 \to D^+\ell^-\bar{\nu}$ decay [14], MM^2, is calculated as,

$$\begin{aligned} MM^2 &= E_\nu^2 - \vec{p_\nu}^2 \\ &= (E_B - (E_{D^+} + E_{\ell^-}))^2 - |\vec{p}_B - (\vec{p}_{D^+} + \vec{p}_{\ell^-})|^2. \end{aligned} \tag{9}$$

The B energy, E_B, is set equal to beam energy, E_{beam}. The B momentum, $\vec{p}_B$, which has a magnitude of about 311 MeV/c, is approximated as zero, because its direction is unknown. Therefore,

$$MM^2 \approx (E_{beam} - (E_{D^+} + E_{\ell^-}))^2 - |\vec{p}_{D^+} + \vec{p}_{\ell^-}|^2 \tag{10}$$

The rms width of the MM^2 distribution is about 0.4 GeV^2, and is dominated by the neglect of $\vec{p}_B$.

This analysis is done in six different four-momentum transfer (q^2) ranges. Because the direction of the B momentum is not known, q^2 cannot be calculated exactly. We use the constraint $MM^2 = 0$ and the known value of $|p_B|$ to find the maximum and the minimum possible value of q^2 for each event which are then averaged to provide a best estimate. (Non-physical values are excluded.) The resolution in q^2 is approximately Gaussian and q^2-dependent, varying from 0.22 GeV^2 to 0.46 GeV^2.

Two general requirements are imposed to select events. The events have to pass hadronic event selection and, in order to suppress continuum background, the ratio of the Fox-Wolfram moments H_2/H_0 must be less than 0.35. As before, the D^+ is reconstructed in the $K^-\pi^+\pi^+$ decay mode, where we require the measured specific ionization for the D^+ daughters to be consistent with the assumed particle hypothesis. The lepton can be either an electron or a muon. All leptons are required to have momentum larger than 1.4 GeV/c, whereas the neutrino reconstruction analysis makes use of electrons with momenta as small as 0.8 GeV/c.

Any event which has ℓ^- and D^+ and passes the cuts described above is potentially a $\bar{B} \to D^+ X \ell^- \bar{\nu}$ event. Multiple candidates are allowed if more than one D^+ candidate is found in the event.

3.2 Backgrounds

The backgrounds to the $\ell^- D^+$ sample are classified in much the same way as in the first analysis described in this paper. We will discuss the backgrounds individually.

3.2.1 Continuum Background

This is a relatively small background. As was described previously, it can be subtracted by examining data taken below the $\Upsilon(4S)$, scaling it to the same luminosity as the on-resonance data sample, correcting for the energy dependence of the cross section, and subtracting it from the on-resonance data.

3.2.2 Combinatoric Background

The combinatoric background arises from random track combinations falling within the D^+ mass peak region. Figure 4 shows the $K^-\pi^+\pi^+$ mass spectrum. To estimate the background under the D^+ peak, we plot the $K^-\pi^+\pi^+$ mass distribution in MM^2 intervals for each q^2 region. We then fit each mass distribution with a D^+ mass signal shape and a background shape. The signal shape is a Gaussian function, and the background shape is a second order polynomial function. The mean and σ of the Gaussian signal shape are obtained as a function of q^2 from the CLEO inclusive $B \to D^+ X$, $D^+ \to K^-\pi^+\pi^+$ data sample. Figure 5 shows the MM^2 distribution summed over all q^2 ranges. The continuum distribution has been subtracted. The combinatoric background in the missing mass analysis is substantially larger than that in the neutrino reconstruction analysis, and therefore requires this more complex treatment.

3.2.3 Fake Lepton Background

The fake lepton background is estimated from data. We repeat the reconstruction procedure except that lepton candidates are now defined as tracks which do not satisfy lepton identification requirements, *i.e.* hadronic tracks. The yield is then scaled by a fake rate factor. In our momentum range, the muon fake rate is about 1.5% per track, while the electron fake rate is about 0.2% per track, for a total fake rate of 1.7% per track.

3.2.4 Uncorrelated Background

As described previously, these are backgrounds in which the D^+ and the lepton are from different B mesons in the event. This background is approximated by using wrong-sign D^+-lepton combinations ($\ell^- D^-$ or $\ell^+ D^+$) in data. The MM^2 distribution for these wrong-sign events is formed exactly as for right-sign combinations. The wrong sign MM^2 spectrum is

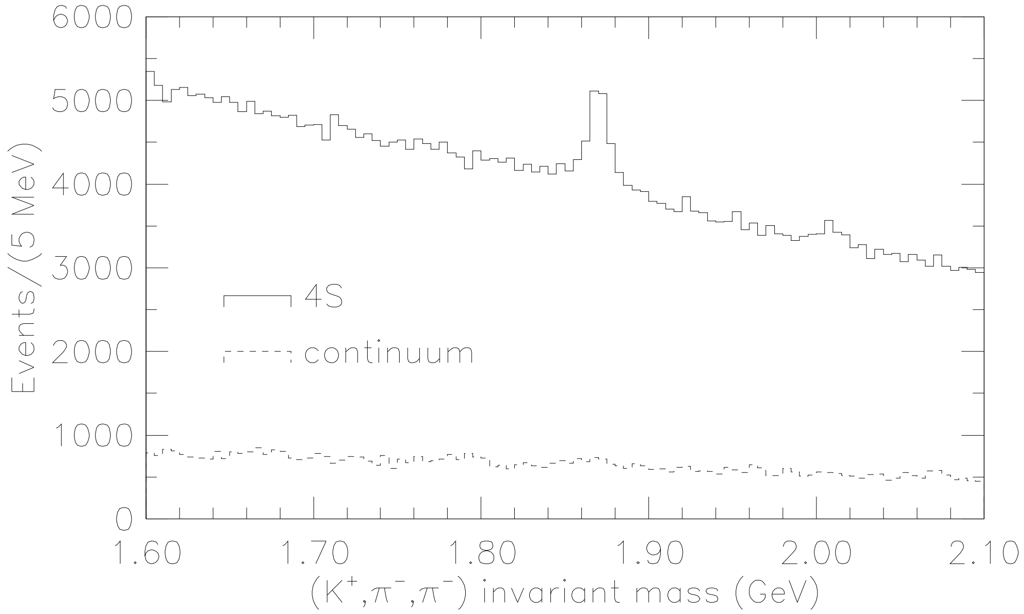

Figure 4: The $K^-\pi^+\pi^+$ invariant mass spectrum for D^+ candidates in events with leptons of momentum greater than 1.4 GeV/c, for both $\Upsilon(4S)$ (solid) and scaled continuum (dashed) events.

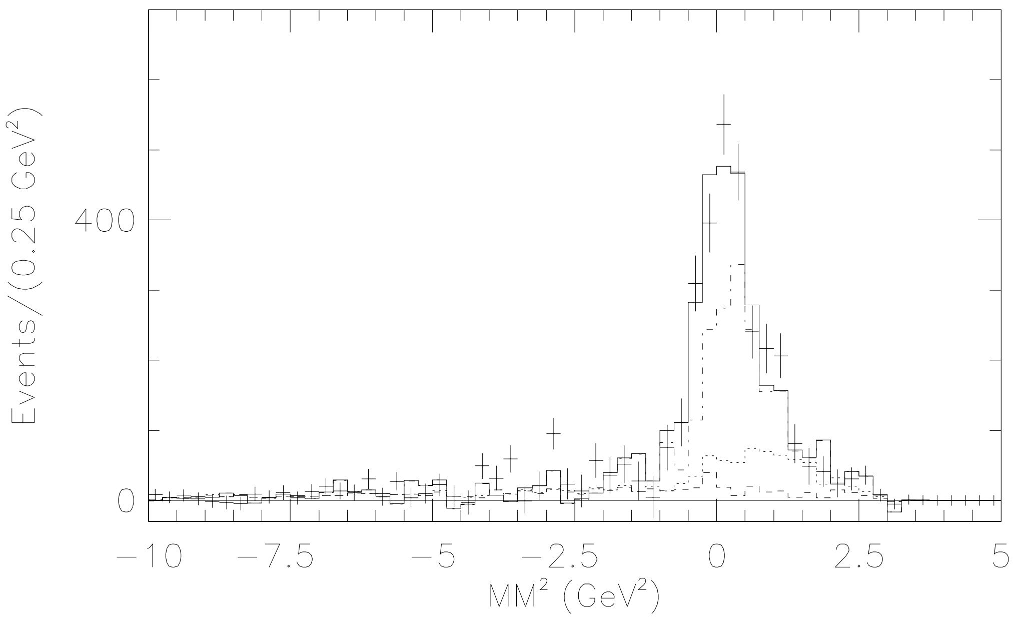

Figure 5: The MM^2 distribution summed over q^2 for all $\ell^- D^+$ events in data. The dashed line is the sum of the contributions from uncorrelated background and fake leptons, the dotted line includes the $D^+ X \ell^- \bar{\nu}$ background, the dot-dash line includes the $D^{*+} X \ell^- \bar{\nu}$ background, and the solid line includes the result of the fit for the signal yield. The contribution from the continuum has been subtracted.

scaled to match the right sign MM^2 spectrum in the region $MM^2 < -3$ GeV^2, where these backgrounds dominate, as shown in Figure 5.

3.2.5 Correlated Background

The second largest background in the MM^2 distribution for $\ell^- D^+$ events is from semileptonic B decays other than $\bar{B}^0 \to D^+\ell^-\bar{\nu}$ which produce D^+ mesons. Poor MM^2 resolution prevents a unique separation of the different semileptonic decays. The most important source of contamination is $\bar{B} \to D^{*+}X\ell^-\bar{\nu}$, $D^{*+} \to D^+\pi^0$. This includes the exclusive $D^{*+}\ell^-\bar{\nu}$ final state. These semileptonic decays where the D^+ arises from a D^{*+} are modeled with data, using events where the D^{*+} is explicitly reconstructed through its decay to $D^+\pi^0$ or $D^0\pi^+$. The shape of the MM^2 distributions is found to be the same for $\ell^- D^0$ pairs from $\bar{B} \to D^{*+}X\ell^-\bar{\nu}$, $D^{*+} \to D^0\pi^+$ and for $\ell^- D^+$ decays from $\bar{B} \to D^{*+}X\ell^-\bar{\nu}$, $D^{*+} \to D^+\pi^0$. The contribution to the MM^2 spectrum from the $B \to D^{*+}Xl^-\bar{\nu}$ background can then be directly subtracted, where a scale factor is used to account for the D^{*+} reconstruction efficiency and the D^{*+} branching fractions. Note that this subtraction does not rely upon the previously measured branching fraction for $\bar{B} \to D^{*+}\ell^-\bar{\nu}$.

The remaining source of correlated background in the MM^2 distribution is semileptonic B decay to higher-spin charm mesons which decay directly to D^+ rather than through D^{*+}. The relevant branching ratios to higher-spin charm mesons are not known, but the MM^2 shape for $\ell^- D^+$ combinations from this background can taken from a Monte Carlo simulation. After all other backgrounds are subtracted we extract the $\bar{B}^0 \to D^+\ell^-\bar{\nu}$ signal by fitting the MM^2 distribution for two components, a $\bar{B}^0 \to D^+\ell^-\bar{\nu}$ signal shape and a background shape, determined in Monte Carlo, to account for higher spin charm mesons or nonresonant $\bar{B} \to D^+X\ell^-\bar{\nu}$ decays.

The contributions to the background summed over all q^2 are shown individually in Figure 5. Figure 6 shows the MM^2 spectrum for all $\ell^- D^+$ events in data summed over q^2 with all of the background distributions subtracted except for the $\ell^- D^+$ events from higher-spin charm mesons that decay directly to D^+ or from non-resonant $D^+n\pi$ final states. That background is estimated by fitting the distribution in each q^2 range, as seen in Figure 7. The normalizations of signal and background components in each q^2 range are independent parameters in the fit. The MM^2 shape for the D^+X background events is quite insensitive to the model used. We fit with the two MM^2 shapes in the restricted range -3 GeV^2 to 3 GeV^2. The first component in the fit is the $D^+\ell^-\bar{\nu}$ component and the second component is the D^+X background. Table 3 shows the raw yield, efficiency and efficiency-corrected yield in each q^2 range. Figure 6 shows the contribution from higher-spin charm mesons summed over all q^2.

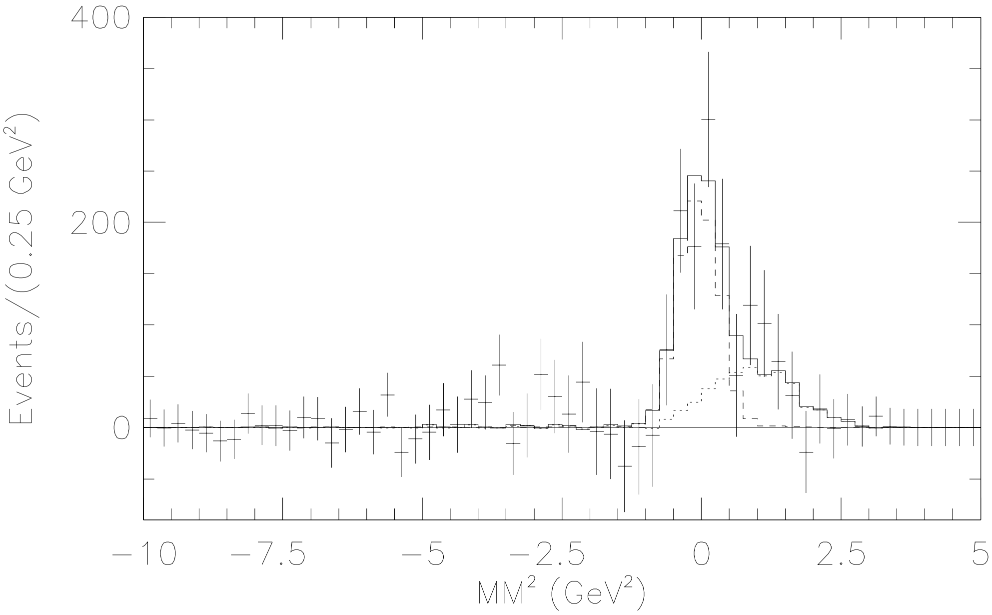

Figure 6: The MM^2 distribution summed over q^2 for $\ell^- D^+$ events in data after all backgrounds from Figure 5 except $D^+ X \ell^- \bar{\nu}$ have been subtracted. The results of the fit to extract the yield are shown. The dashed line is the signal component and the dotted line is the D^{**} background. The solid line is the sum of the signal and the D^{**} background.

Table 3: $\bar{B}^0 \to D^+ \ell^- \bar{\nu}$ yields from the missing mass analysis.

q^2 range (GeV^2)	Raw Yield	Efficiency (%)	Yield
$0-2$	247 ± 46	10.46	2365 ± 436
$2-4$	265 ± 44	12.44	2126 ± 355
$4-6$	194 ± 61	13.43	1445 ± 453
$6-8$	179 ± 77	18.13	985 ± 426
$8-10$	-18 ± 92	23.03	-77 ± 401
$10-12$	0 ± 124	38.37	-1 ± 322

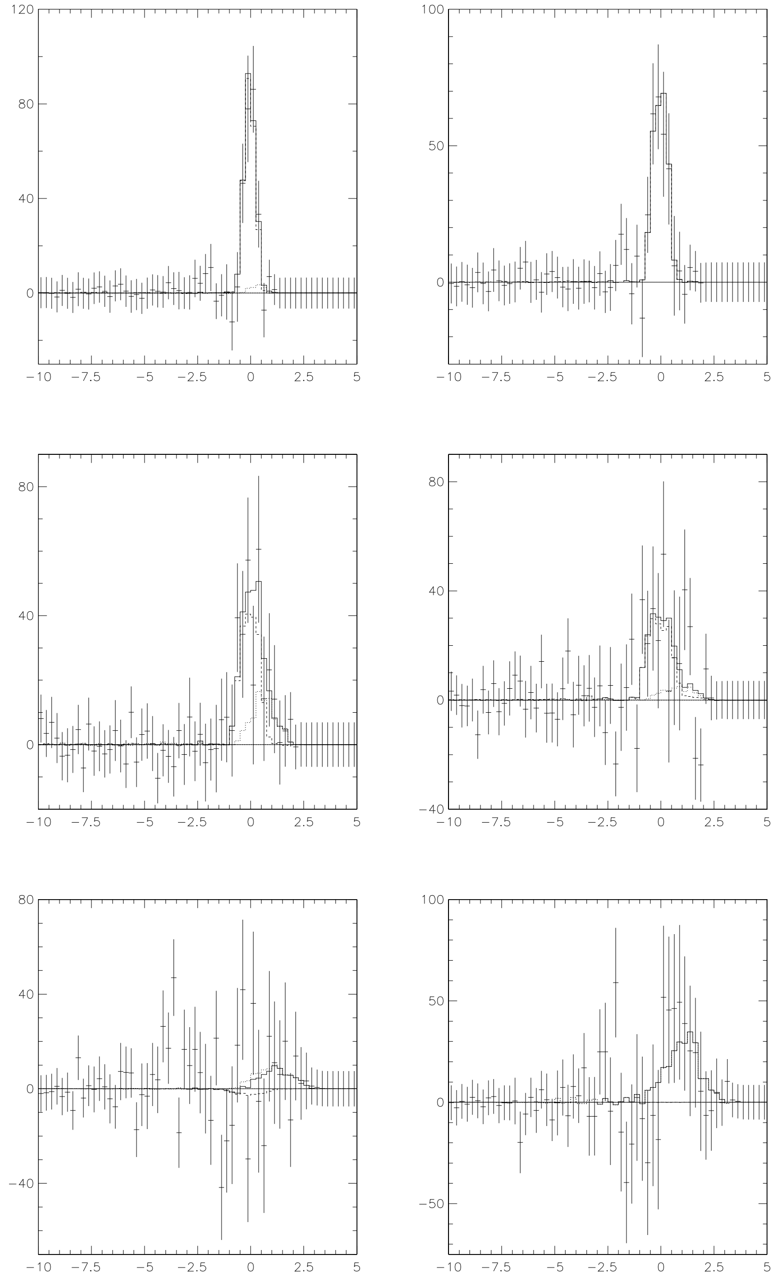

Figure 7: The MM^2 distribution in each q^2 range for D^+-lepton events after all backgrounds have been subtracted. Each distribution contains a range of 2 GeV^2 in q^2, with q^2 increasing from left to right and from top to bottom in the figure. The results of the fit to extract the yield are shown. The dashed line is the signal component and the dotted line is the D^{**} background. The solid line is the sum of the signal and the D^{**} background.

Table 4: Systematic errors on $\mathcal{B}(\bar{B}^0 \to D^+\ell^-\bar{\nu})$ in the missing mass analysis.

Source	Error
Tracking efficiency	6.0%
$D^{*+}X\ell^-\bar{\nu}$ background	2.9%
Other backgrounds	3.0%
Efficiency	8.1%
D branching ratio	6.6%
Total	11.3%

3.3 Results

3.3.1 Branching Ratio

The branching ratio for $\bar{B}^0 \to D^+\ell^-\bar{\nu}$ in each q^2 range is given by

$$\Delta\mathcal{B}(\bar{B}^0 \to D^+\ell^-\bar{\nu}) = \frac{\Delta N}{2.153 \times 10^6 \cdot \mathcal{B}(D^+ \to K^-\pi^+\pi^+) \cdot 2}, \tag{11}$$

and $\mathcal{B}(\bar{B}^0 \to D^+\ell^-\bar{\nu})$ is given by

$$\mathcal{B}(\bar{B}^0 \to D^+\ell^-\bar{\nu}) = \sum_{q^2\ ranges} \Delta\mathcal{B}(\bar{B}^0 \to D^+\ell^-\bar{\nu}) \tag{12}$$

Using $\mathcal{B}(D^+ \to K^-\pi^+\pi^+) = (9.1 \pm 0.6)\%$ we extract

$$\mathcal{B}(\bar{B}^0 \to D^+\ell^-\bar{\nu}) = (1.75 \pm 0.25 \pm 0.20)\% \tag{13}$$

where the first error is statistical and the second is systematic. Systematic errors are summarized in Table 4.

3.3.2 Extraction of $|V_{cb}|$ in the Heavy Quark Limit

This proceeds in the same fashion as for the previously described technique. The fit to the dN/dw distribution is shown in Figure 8. We find:

$$|\mathcal{F}(1)V_{cb}| = (3.25 \pm 0.60 \pm 0.53) \times 10^{-2} \tag{14}$$

$$\rho^2 = 0.52 \pm 0.29 \pm 0.10. \tag{15}$$

Again, an alternative approach to extracting $|V_{cb}|$ is to fit the $d\Gamma/dq^2$ distribution for $|V_{cb}f_+(q^2)|$ where the q^2 dependence of the form factor and its normalization are predicted from a model calculation. At $q^2 = 0$, we obtain a value $|V_{cb}f_+(0)| = (2.60\pm0.18\pm0.16)\times10^{-2}$.

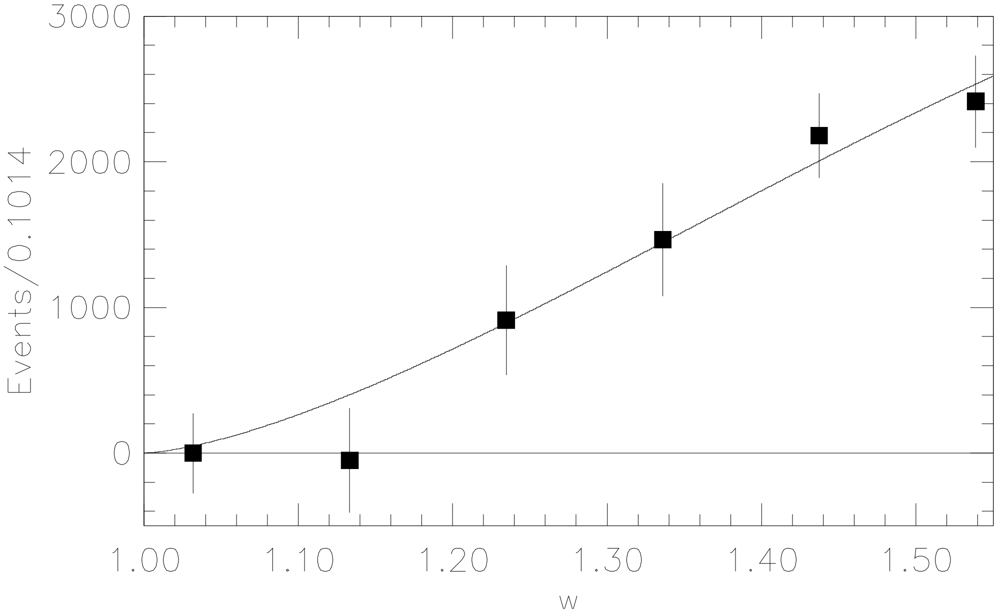

Figure 8: The result of the fit of dN/dw from the missing mass analysis.

4 Conclusions

The results of the two analyses are in excellent agreement. The statistical errors are essentially uncorrelated because the events that are common to both analyses are a small fraction ($\mathcal{O}(1\%)$) of the events in the missing mass analysis. The results of the two methods can be combined. Pending a careful study of correlations between the errors in the two analyses, we assume that the systematic errors are entirely correlated. Our preliminary result is

$$\mathcal{B}(\bar{B}^0 \to D^+\ell^-\bar{\nu}) = (1.78 \pm 0.20 \pm 0.24)\%$$

Similarly, we combine the results of the fits to the differential decay distributions to extract

$$|\mathcal{F}(1)V_{cb}| = (3.46 \pm 0.42 \pm 0.46) \times 10^{-2} \tag{16}$$

$$\rho^2 = 0.64 \pm 0.18 \pm 0.10. \tag{17}$$

Figure 9 shows $|\mathcal{F}(w)V_{cb}|$ with the parameters that we have determined by combining the two analyses. The points are our measured values of $|\mathcal{F}(\tilde{w})V_{cb}|$ from the two analyses. (Note that the curve is *not* a direct fit to the points shown, but is obtained from the results of the two analyses.)

In the heavy quark limit, this would be a measurement of $|\xi(w)V_{cb}|$, which would be the same for both $B \to D\ell\nu$ and $B \to D^*\ell\nu$ decays because of the spin-flavor symmetry of HQET. Figure 9 also shows (as a dashed line) $|\mathcal{F}(w)V_{cb}|$ as measured in $B \to D^*\ell\nu$ decays [8]. Our result is in agreement with this measurement.

Note, however, that we are not in the heavy quark limit, and therefore $\mathcal{F}(1)$ is not necessarily the same for $D\ell\nu$ and $D^*\ell\nu$. Using a value of $\mathcal{F}(1)$ from Caprini and Neubert [15], for instance, of $\mathcal{F}_{D^+\ell^-\bar{\nu}}(1) = 0.98 \pm 0.07$ we find

$$|V_{cb}| = (3.53 \pm 0.46 \pm 0.44 \pm 0.25) \times 10^{-2}, \tag{18}$$

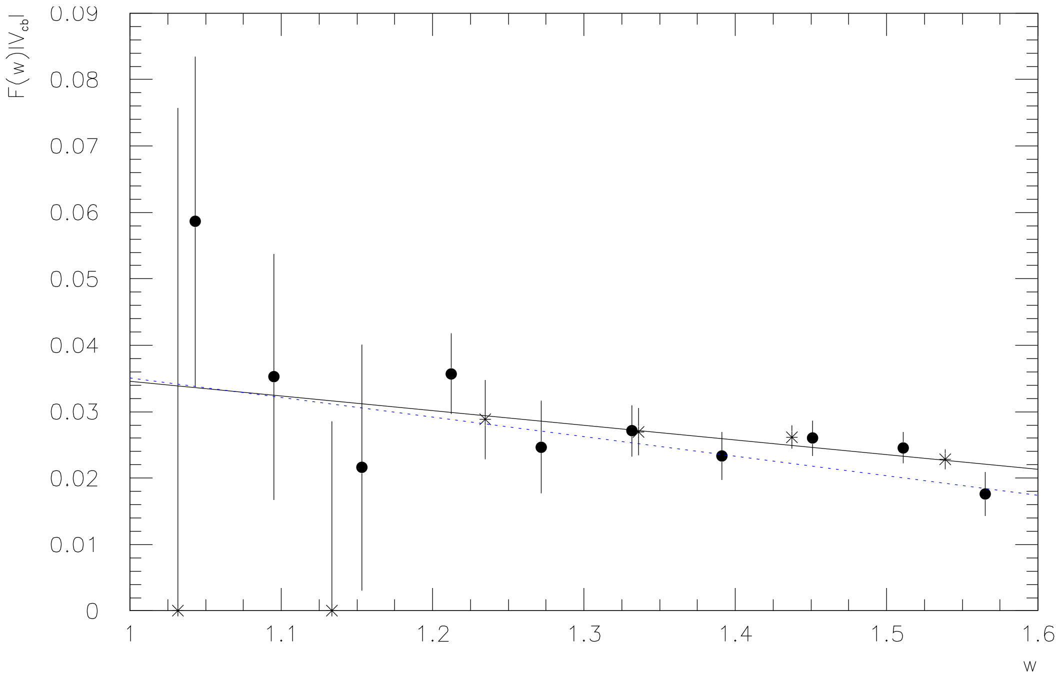

Figure 9: Measured values of $|\mathcal{F}(\tilde{w})V_{cb}|$ with the results from the neutrino reconstruction analysis (solid dots) and the missing mass analysis (asterisks) with the combined results shown as the solid line. Note that the curve shown is *not* a fit to the points shown. The dashed line denotes $\mathcal{F}(w)$ as measured in $B \to D^*\ell\nu$ decays [8].

Table 5: $|V_{cb}|$ as extracted using form factor predictions of models.

Model	Prediction	$\lvert V_{cb}\rvert \times 10^2$
WSB [17]	$f_+(0) = 0.69$	$3.73 \pm 0.20 \pm 0.25$
KS [18]	$f_+(0) = 0.7$	$3.67 \pm 0.20 \pm 0.24$

where the last error is the uncertainty due to $\mathcal{F}(1)$. This value is in good agreement with the value of $|V_{cb}| = (3.88 \pm 0.20(\text{exp}) \pm 0.12(\text{theory})) \times 10^{-2}$ determined in $D^*\ell\nu$ decays [16].

Values of $|V_{cb}|$ can also be obtained from $|V_{cb}f_+(0)|$ and predictions for $f_+(0)$ obtained by various models. Combining the results of the two analyses, we find

$$|V_{cb}f_+(0)| = (2.57 \pm 0.14 \pm 0.17) \times 10^{-2}. \tag{19}$$

Table 5 gives values of $|V_{cb}|$ obtained from different models using this value. They are in agreement with $|V_{cb}|$ as obtained from the heavy quark limit.

Alternatively, we can use our measured values of $|\mathcal{F}(1)V_{cb}|$ and $|V_{cb}f_+(0)|$ and a value of $|V_{cb}|$ [16] to obtain values for $\mathcal{F}(1)$ and $f_+(0)$. We find $\mathcal{F}(1) = 0.89 \pm 0.16 \pm 0.05$ and $f_+(0) = 0.66 \pm 0.06 \pm 0.04$, where the first error is from our measurements and the second error is from the value of $|V_{cb}|$.

Finally, we can use the measured q^2 dependence of the $\bar{B}^0 \to D^+\ell^-\bar{\nu}$ decay to test the hypothesis of factorization. In semileptonic decays, the decay amplitude "factorizes" into

Table 6: Results of factorization tests, assuming $a_1 = 1$.

h	$d\mathcal{B}/dq^2\|_{q^2=m_h^2}$ (%/GeV^2)	R_{th} (GeV^2)	R_{exp} (GeV^2)	R_{exp}/R_{th}
π	$0.35 \pm 0.04 \pm 0.04$	0.98 ± 0.01	0.83 ± 0.20	0.85 ± 0.20
ρ	$0.33 \pm 0.04 \pm 0.04$	2.60 ± 0.04	2.45 ± 0.66	0.94 ± 0.25

separate leptonic and hadronic parts, because the leptons are not affected by the strong interaction. The factorization hypothesis suggests that two-body hadronic B decays can be treated in the same manner, with one hadronic current governing the formation of the charm meson, and another governing the hadronization of the virtual W. This can be tested by comparing the decay rates for two-body hadronic states with the decay rate for a semileptonic decay at the appropriate q^2. According to the factorization hypothesis,

$$\frac{\mathcal{B}(\bar{B}^0 \to D^+ h^-)}{d\mathcal{B}/dq^2(\bar{B}^0 \to D^+\ell^-\bar{\nu})|_{q^2=m_h^2}} = 6\pi^2 a_1^2 f_h^2 |V_{ud}|^2. \tag{20}$$

The left hand side of the equation is referred to as R_{exp}, and the right hand side is known as R_{th}.

Table 6 gives results for $d\mathcal{B}/dq^2$ at two different q^2 points from combining the results of these two analyses, and the corresponding values of R_{exp} and R_{th} and their ratio which have been determined using parameters given in Reference 19, and assuming $a_1 = 1$. In both cases, R_{exp} and R_{th} are in good agreement.

We gratefully acknowledge the effort of the CESR staff in providing us with excellent luminosity and running conditions. J.P.A., J.R.P., and I.P.J.S. thank the NYI program of the NSF, M.S thanks the PFF program of the NSF, G.E. thanks the Heisenberg Foundation, K.K.G., M.S., H.N.N., T.S., and H.Y. thank the OJI program of DOE, J.R.P, K.H., and M.S. thank the A.P. Sloan Foundation, and A.W., and R.W. thank the Alexander von Humboldt Stiftung for support. This work was supported by the National Science Foundation, the U.S. Department of Energy, and the Natural Sciences and Engineering Research Council of Canada.

References

[1] *B Decays*, ed. S. Stone, World Scientific, Singapore (1994).

[2] J. D. Richman and P. R. Burchat, Rev. Mod. Phys **67**, 893, 1995.

[3] R. Fulton *et al.*, Phys. Rev. **D43**, 651 (1991); H. Albrecht *et al.*, Phys. Lett. **B229**, 175 (1989).

[4] Y. Kubota *et al.*, CLEO-CONF-95-10, paper submitted to 17th Lepton and Photon Interactions Symposium, Beijing, China (1995); R. A. Briere, contribution to the 31st Recontres de Moriond, Les Arcs, France, March 1995; L. Di Ciaccio, *loc cit.*

[5] Here and throughout the paper, charge conjugate modes are implied.

[6] Y. Kubota *et al.*, Nucl. Instrum. Methods **320**, 66 (1992).

[7] G. Fox and S. Wolfram, Phys. Rev. Lett. **41**, 1581 (1978).

[8] B. Barish *et al.*, Phys. Rev. **D51**, 1014 (1995).

[9] N. Isgur, D. Scora, B. Grinstein, and M.B. Wise, Phys. Rev. **D39**, 799 (1989).

[10] R. Brun *et al.*, GEANT v. 3.14, CERN Report No. CERN DD/EE/84-1 (unpublished).

[11] Particle Data Group, L. Montanet *et al.*, Phys. Rev. **D50**, 1173 (1994).

[12] N. Isgur and M. Wise, Phys. Lett. **B232**, 113 (1989); Phys. Lett. **B237**, 527 (1990); E. Eichten and B. Hill, Phys. Lett. **B234**, 511 (1990); H. Georgi, Phys. Lett. **B240**, 447 (1990).

[13] In the fit, $\chi^2 = 4.5$ for 8 degrees of freedom, and the correlation coefficient is 0.94.

[14] Note the difference between MM^2 defined here and MM^2_{EV}, the missing mass squared of the entire event used in the neutrino reconstruction procedure.

[15] I. Caprini and M. Neubert, CERN-TH/95-255.

[16] M. Neubert, "B Decays and CP Violation," CERN-TH/96-55.

[17] M. Wirbel, B. Stech, and M. Bauer, Z. Phys. C **29**, 637 (1985); M. Bauer and M. Wirbel, Z. Phys. C **42**, 671 (1989).

[18] J.G. Korner and G.A. Schuler, Z. Phys. C **38**, 511 (1988); J.G. Korner and G.A. Schuler, Z. Phys. C **41**, 690 (1989) (erratum).

[19] M.S. Alam *et al.*, Phys. Rev. **D50**, 43 (1994), Section X and references therein.